Optimizing Injected Dose in Clinical PET by Accurately Modeling the Counting-Rate Response Functions Specific to Individual Patient Scans

Charles C. Watson, PhD[1]; Michael E. Casey, PhD[1]; Bernard Bendriem, PhD[1]; Jonathan P. Carney, PhD[2]; David W. Townsend, PhD[3]; Stefan Eberl, PhD[4]; Steve Meikle, PhD[4]; and Frank P. DiFilippo, PhD[5]

[1]Siemens Medical Solutions Molecular Imaging, Knoxville, Tennessee; [2]Department of Radiology, University of Pittsburgh, Pittsburgh, Pennsylvania; [3]Graduate School of Medicine, University of Tennessee Medical Center, Knoxville, Tennessee; [4]PET and Nuclear Medicine Department, Royal Prince Alfred Hospital, Camperdown, New South Wales, Australia; and [5]Department of Molecular and Functional Imaging, Cleveland Clinic Foundation, Cleveland, Ohio

To optimize the injected dose of radiopharmaceutical in PET, one needs to know its relationship to some metric of data quality for individual patient scans, such as noise-equivalent counting rate (NECR). In this paper, we show how one may accurately model the clinical NECR response corresponding to specific patient scans much as if a counting-rate test had been performed on each patient. We apply this technique to patient data and show how it can lead to improved clinical scanning protocols. **Methods:** True and random coincidence rates expressed as functions of an appropriate measurable system parameter such as the detector single-event rate have functional forms that are largely independent of the object being scanned. Thus, reference true and random response functions may be scaled directly to the specific counting rates measured on a clinical scan, thereby yielding a curve of NECR versus injected dose. We have applied this technique to 2 groups of 163 clinical ^{18}F-FDG scans each. One of the groups was obtained on a lutetium oxyorthosilicate PET/CT scanner with conventional front-end electronics, and the other was obtained on a lutetium oxyorthosilicate PET/CT scanner with a new digital data processing system (Pico-3D). **Results:** At 90%–95% of maximum signal-to-noise ratio (SNR), the mean optimal dose for a 60-min uptake period ranged from 366 to 717 MBq depending on the electronics and randoms processing method. There was only a slight (1 MBq/kg) dependence of optimal dose on patient weight but a larger dependence on position in the body. Pico-3D electronics improved optimal data SNR by 35% for a 70-kg person, but in both cases NECR fell rapidly with increasing weight (1.4%/kg). For an equivalent data SNR, a 120-kg person would have to be scanned 2.3 times longer than a 60-kg person. Over this range of weight, the mean scatter fraction increased by 12% whereas the ratio of mean randoms to trues increased by 48%. **Conclusion:** The methodology developed here allows one to directly estimate the optimal dose to inject for specific clinical scans and permits a detailed analysis of the sources of noise in PET data and of their variation with parameters such as patient weight.

Key Words: PET; noise equivalent counting rate; optimal injected dose; clinical data quality

J Nucl Med 2005; 46:1825–1834

Because nuclear positron emission is a Poisson-distributed random process, PET is a statistical imaging technique with unavoidable noise in the true coincidence data and resulting images. It seems natural to try reducing this noise by injecting the patient with greater amounts of radiopharmaceutical to increase the counting rate. However, the statistical quality of this coincidence data per unit scan time, typically characterized by the noise-equivalent counting rate (NECR) (*1*), is generally not a simple monotonic function of activity in the patient and usually exhibits a peak. This is illustrated in Figure 1, which shows some examples of estimated NECR versus injected dose (D_{inj}) of ^{18}F-FDG for a whole-body patient scan. D_{inj} is proportional to the activity in the patient. The falloff in performance at higher activities is due to increasing counting losses and accidental coincidences.

To minimize the relative data variance in clinical PET scans by adjusting D_{inj}, one needs to know the NECR(D_{inj}) response curve for the patient. Unfortunately, this curve is not a universal function, even for a specific scanner, and varies widely between patients and with position in the body, as demonstrated in Figure 1. It would be difficult to measure NECR(D_{inj}) directly in humans both because they would poorly tolerate the long scanning periods required, at least for ^{18}F-FDG (110-min half-life), and because activity redistributes within the body over time. Thus, some indirect means of determining the counting-rate response is required.

Received Jan. 18, 2005; revision accepted Jun. 13, 2005.
For correspondence or reprints contact: Charles C. Watson, PhD, CPS Innovations, 810 Innovation Dr., Knoxville, TN 37932-2571.
E-mail: Charles.Watson@cpspet.com

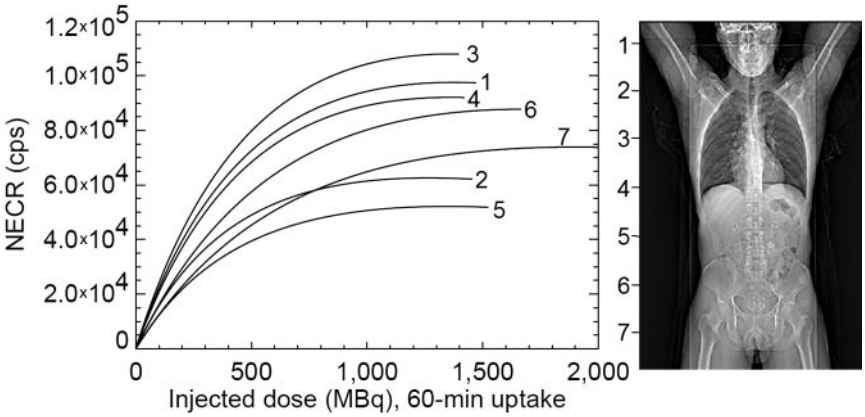

FIGURE 1. Examples of NECR response vs. D_{inj} for 7 bed positions in clinical whole-body ^{18}F-FDG examination performed on Pico-3D LSO PET/CT scanner. Each tick mark along left edge of x-ray projection image indicates center of bed position to which indicated response curve corresponds.

NECR response analysis has been widely used to characterize the performance of PET tomographs for clinical scanning (*2–5*). In these studies, NECR versus activity is typically determined from simulations or measurements on phantoms that are more or less bodylike, and the results are extrapolated to humans. Indeed, the National Electrical Manufacturers Association (NEMA) NU 2-2001 standard (*1*) includes a counting-rate measurement on a 20-cm-diameter, 70-cm-long cylinder that is suggested to provide a reasonable characterization of whole-body performance (*6*). However, the NECR response in humans is actually quite varied, and it is not feasible to characterize this variability with only one or a few simulations or measurements. Nor is it easy to understand how representative a phantom study might be of a patient population or to directly relate such a study to any particular patient. Badawi et al. (*7*) partially addressed these issues by performing simulations on numeric phantoms based on 3 actual patient images. Trying to relate phantom and clinical studies, Smith and Karp (*8*) showed a correlation for the prompts and trues rates as a function of singles rates between patient data and standard phantom measurements but did not evaluate NECR performance. More recently, Lartizien et al. (*9*) have developed a methodology to evaluate patient data in terms of NECR. Their approach differs from ours in at least 2 important ways. They model patient response based on counting-rate curves for prompts and randoms rather than trues and randoms. More important, they do not attempt to scale counting-rate curves to individual patient scans but instead use measurements obtained from an anthropomorphic phantom to derive fixed models for the prompt and delayed coincidence rates as a function of singles rates, relying on the similarity between the phantom and patients, as many authors have done previously. The applicability of these results to more extended patient populations has not been demonstrated.

We have previously pointed out that counting-rate responses in human subjects could accurately be estimated simply by scaling true and random coincidence rate functions measured in phantoms to the corresponding data points from individual clinical scans (*10*). This works for basically the same reason that it is possible to correct patient data for counting losses, namely that counting losses are uniquely determinable from some measurable parameter such as the single-event rates in the scanner's detectors and do not otherwise depend on the object being scanned. With this approach, we could approximate a measure of NECR as a function of singles rate or D_{inj} in the patient. The pseudo-NECR used for this analysis did not accurately account for variations in the fractions of the scatter and random events that are internal to the patient, however, because these data were not available from clinical reconstruction software at the time. These values are reported in current systems (*11*), making it possible now to estimate actual NECR versus counting rate for patients.

The present paper expands this previous work by using clinical counting-rate modeling together with accurate scatter and randoms estimates to predict true NECR response functions for each individual scan in 2 groups of patient studies. This technique not only permits us to determine the D_{inj} that would have been optimal for that scan but also allows us to meaningfully evaluate the effect of patient parameters, such as weight, on system performance without the confounding uncertainty of arbitrarily varying activity level. Analysis of the individual components contributing to the noise can help shed light on certain well-known but poorly understood phenomena such as the inevitable degradation of PET image quality with increasing patient weight. We also demonstrate the effect of varying scanner performance characteristics by presenting results from 2 different PET/CT scanners: the lutetium oxyorthosilicate (LSO) PET/CT and the LSO PET/CT with Pico-3D digital electronics (both products of Siemens Molecular Imaging).

MATERIALS AND METHODS

Signal-to-Noise Ratio (SNR) of PET Data

The measure we use for selecting optimal D_{inj} is the global SNR of the total true coincidence rate (T) summed over lines of response (LORs) passing through the patient, defined as:

$$SNR_{data} = T/\sigma_T, \qquad \text{Eq. 1}$$

where σ_T is the SD of T. $T = P - S - R$, where P is the prompt coincidence rate; R is the delayed coincidence, or randoms, rate; and S is the rate of scattered coincidence events, all evaluated as sums over the internal LORs. Under the assumption that the measured prompts and randoms are Poisson distributed and uncorrelated, SNR_{data} is related to NECR by (*12*):

$$SNR^2_{data} = [T^2/(P + kR)]\Delta t$$
$$= [T^2/(T + S + (k + 1)R)]\Delta t = \text{NECR}\ \Delta t, \quad \text{Eq. 2}$$

where Δt is the duration of the acquisition. For LSO-based systems, there is a small contribution from intrinsic trues arising from the natural radioactivity of ^{176}Lu that is neglected here. For the systems we discuss, scatter is estimated by means of simulation from preliminary images (*11*). Although the resulting scatter sinogram is not completely noise free, it is always much smoother than the measured data, and we neglect its contribution to the corrected trues variance. The factor k depends on how the randoms are estimated. As a practical matter on clinical systems, k would fall somewhere between 0 and 1. It would be closer to 0 if randoms were computed from detector singles rates or smoothed delayed sinogram data and closer to 1 if the delayed sinogram were used without smoothing or interpolation. Because optimal dose, as well as peak SNR_{data}, can depend significantly on this term, we present results for the 2 extreme cases. We refer to the $k = 0$ case as $1R$ and the $k = 1$ case as $2R$. T and R in Equation 2 should be expected mean rates; for reporting clinical results, we approximate these by the measured, sample rates.

Although NECR is an accepted metric for PET integral data precision (*1,6*), it has some potential deficiencies. The sinogram data may not actually be Poisson because of effects such as detector dead time (*13*), weighted rebinning, or interpolation. A statistical measure such as NECR does not account for possible counting-rate–dependent bias such as the systematic mispositioning of data because of spatial pile-up effects (*14*). Nor does NECR account for the normalization, attenuation correction, or reconstruction of the data. A local SNR of the reconstructed image that does account for these latter effects can be derived, however, and it has been shown (*12*) that for filtered backprojection reconstruction of Poisson data, global NECR response accurately tracks the local SNR of clinical PET images versus D_{inj}, except perhaps in the immediate vicinity of regions of high activity, such as the bladder. Good correlation between NECR and image noise in uniform cylinders has also been shown for ordered-subset estimation maximization reconstruction as well as filtered backprojection, using statistical sampling techniques (*15*). Thus, despite its limitations, NECR seems to be a useful measure for characterizing the major factors in the counting-rate dependence of image noise for an individual patient.

It is less clear how NECR and image SNR are quantitatively related across different patients, in whom parameters such as weight may be varying. For example, heavier patients have larger volumes and thus, at equal NECR, could exhibit lower count densities than do lighter patients in regions that affect image quality. This issue requires further study of local SNR that is beyond the scope of the present paper. Further, the relationship between local SNR and image quality has no unique definition. Thus, we do not claim to be addressing here the relationship between D_{inj} and final image quality but only between dose and data quality. On the other hand, the modeling technique developed in this paper is not limited to NECR but could be applied to a more comprehensive measure of image quality as well, should one be defined.

Counting-Rate Modeling

To estimate the dependence of SNR_{data} on D_{inj} for a patient, one needs to model the counting rates as functions of activity in the body or some quantity related to it. Although the prompts and randoms rates are the ones that are directly measured, the fundamental rates for modeling purposes are the trues and randoms, because of their distinct functional dependence on the activity.

If there were no counting losses in the system and no intrinsic detector activity, then regardless of the distribution of the emitter and attenuating medium, the trues rate, $T(a)$, would vary linearly with a, whereas $R(a)$ would be nearly proportional to a^2, where a is the amplitude of a fixed spatial distribution of activity in the patient. In this case it would be simple to scale T and R to any activity level if they were known at 1 value of a. In practice, clinical systems experience significant and unavoidable counting losses that are due both to pulse processing at the detector (dead time and pile-up) and to multiplexing of the data channels from the detectors to the coincidence processor. These losses are nonlinear functions of the photon flux incident on the detectors, whose relationship to the activity present depends on the configuration of the emitter and attenuation distributions. Consequently, the shapes of $T(a)$ and $R(a)$ become dependent on the object being scanned, and a simple scaling based on the measured T and R rates is not possible. It is therefore necessary to characterize the counting-rate models in terms of a measurable system parameter such that the losses depend solely on this parameter and not on the structure of the scanned object.

The incident photon flux is not directly known, of course, but the output single-event rates of the detectors are measured and recorded on many PET systems. If the losses depend essentially only on the number of incident photons per second and not on other properties, such as their angular or energy distribution, then these measured single-event rates may be adequate to characterize the response of the system. This is, in fact, the basis of count-loss corrections on many PET systems, which compute a loss factor for any pair of detectors as a function of the singles rates recorded by them. An assumption here is that a monotonic relationship exists between the measured single-event rate and the incident flux, or the activity present, over the clinical range of interest. This will certainly be the case if the detectors are not paralyzable (which is true for the systems we discuss here). Although some scanners may not provide information on singles rates, all clinical systems afford some means of making count-loss corrections based on a measurable quantity that should be suitable to use as a parameter for counting-rate models. For example, the use of measured "detector dead time" for this purpose has been reported (*16*).

In principle, a counting-rate model as a function of all the individual detector singles rates could be developed but, for the systems we have examined, does not seem to be necessary. Instead, we use the integral singles rate, s, summed over all detectors. The justification for characterizing the loss functions for the integral coincidence rates T and R in terms of the integral singles rate comes from validation in a wide range of phantom studies (*10,12*) and has been explained as a consequence of the moderate variation in singles rates among detectors in clinical scans (*12*).

In terms of activity, the integral trues, randoms, and singles rates can be expressed in the form:

$$T(a) = c_T a f_T[s(a)]$$
$$R(a) = c_R(a + a_{int})^2 f_R[s(a)]$$
$$s(a) = (c_s a + s_{int}) f_s[s(a)], \quad \text{Eq. 3}$$

where c_T, c_R, and c_s are object-dependent constants, s_{int} is the object-independent intrinsic singles rate (for LSO systems), a is the activity amplitude, $a_{int} = s_{int}/c_s$ is the external equivalent of the internal ^{176}Lu activity, and f_T, f_R, and f_s are object-independent live-time fractions for the rates of trues, randoms, and singles, respectively. We define $f_s(s_{int})$ to be equal to 1. We neglect a small intrinsic contribution to the trues. Although in principle the losses for an individual event do not depend on whether the event eventually contributes to a true or random coincidence, differing sensitivities for contributions to T and R can cause slight differences in $f_T(s)$ and $f_R(s)$ when coincidence events are summed over multiple detector pairs.

Equation 3 can be inverted to give T, R, and a as functions of the singles rate (assuming $s(a)$ is monotonic):

$$T(s) = \frac{c_T}{c_s}\left[\frac{s}{f_s(s)} - s_{int}\right] f_T(s)$$
$$R(s) = \frac{c_R}{c_s^2}\left[\frac{s}{f_s(s)}\right]^2 f_R(s)$$
$$a(s) = \frac{1}{c_s}\left[\frac{s}{f_s(s)} - s_{int}\right]. \quad \text{Eq. 4}$$

Thus, $T(s)$, $R(s)$, and $a(s)$ can be expressed as object-independent functions of s, multiplied by object-dependent scale factors. These functional forms can be determined from phantom measurements and then simply scaled to patient data to yield the clinical counting-rate response curves versus s. $T(a)$ and $R(a)$ can then be evaluated by numerically transposing $a(s)$ to get $s(a)$ and substituting.

In principle, the scatter event rate, S, should be modeled independently of T since the scatter fraction of the data $S_f = S/(T + S)$ may vary with counting rate because of energy or spatial pile-up or because of other effects. In practice, S_f has been observed to increase by only a few percentage points as the counting rate increases over the operational range of the scanners we use (*17,18*), and we have chosen to neglect its variation. In fact, because the directly measurable counting rate is $T + S$ (prompt minus delayed coincidences) whereas S must be estimated, we actually model $T + S$ rather than T itself as a function of the singles counting rate and then compute the trues from $T = (1 - S_f)(T + S)$.

The randoms, trues, and singles live-time functions could be expressed in terms of the fundamental detector and multiplexing loss processes and theoretic forms used to model them. A simpler and arguably more accurate approach is to model $(T + S)(s)$, $R(s)$, and $a(s)$ directly. We follow this approach and fit second- or third-order polynomial functions to phantom counting-rate data to determine our model functions. For this purpose, we typically use the NEMA NU 2-2001 70-cm-long phantom (*1*), but other common phantoms will work as well.

In the case of a stationary phantom with a fixed distribution of activity, $T(a)$ and $R(a)$ would be equivalent to counting-rate functions measured as the radioactivity decayed, but in discussing clinical counting-rate curves we are actually considering hypothetical variations in the amplitude of a for a fixed spatial distribution within the patient. Because the actual activity in the patient is not known, however, we characterize response in terms of the D_{inj}, which will be proportional to the activity to the extent that uptake and excretion of activity are constant factors. Thus, $T(D_{inj})$ and $R(D_{inj})$ represent expected results for an ensemble of scans of a patient differing only in the amount of radiopharmaceutical initially injected. To avoid extraneous variability due to differing uptake periods and scan durations, we standardize the D_{inj} of ^{18}F-FDG to an equivalent effective dose, D_{inj}^{60}, which would give the same initial total activity in the patient after a 60-min uptake as the actual average activity present during the scan. If t_{up} is the actual uptake period to the beginning of the acquisition, and τ is the mean life ($\tau \ln 2 = t_{1/2}$, where $t_{1/2}$ is the half-life) of the isotope (both in minutes), then:

$$D_{inj}^{60} = D_{inj}\frac{\tau}{\Delta t}(1 - e^{-\Delta t/\tau})e^{-(t_{up}-60)/\tau}. \quad \text{Eq. 5}$$

We compute a distinct effective dose for each acquisition; in particular, for each bed position in a whole-body scan. The effective dose does not account for any redistribution of activity that might occur between the actual and standard uptake periods or the possible effect of excretion of part of the dose before scanning. These factors are not an issue for characterizing the SNR_{data} response of an individual patient, but they could possibly confound results in population studies if they were correlated with characteristics of interest such as weight. In the results presented here, we are not aware of any such correlations; however, we do not control for these factors.

Estimation of Scatter, Randoms, and Trues

Computation of NECR requires accurate estimates of the trues, scatter, and random counts lying within the patient—that is, on LORs passing through the body. To compute the scatter, we use an implementation of the single scatter simulation algorithm (*11*), which accurately estimates its nonuniform spatial distribution both within and outside the patient. As part of this algorithm, a sinogram mask defining the interior of the patient is formed by applying a threshold of 1.1 to the attenuation correction factor sinogram. This mask (actually, its complement) is used to define a region for scaling the estimated scatter to the measured emission data in order to account for the contribution of activity outside the field of view. The mask is then applied to the scaled scatter sinogram to derive S, applied to the net trues sinogram (prompt minus delayed coincidences) to estimate $T + S$, and applied to the randoms sinogram to estimate R for the calculation of NECR. When online subtraction of randoms is used, no randoms sinogram is acquired, and we assume a uniform distribution of the random coincidences for the purpose of estimating the internal randoms fraction. This is the procedure followed for the clinical examples presented here. In fact, however, the distribution of random events in the sinogram is generally not uniform and may vary by a factor of 2 or more. On the other hand, in these cases the patient tends to take up a large fraction (65%–75%) of the sinogram. We have therefore evaluated the potential error incurred by the assumption of uniformity by estimating randoms sinograms from the measured detector singles rates for 10 of the studies discussed here. Applying the internal patient mask to these estimated nonuniform randoms sinograms, we find less than 2% deviation in the estimated randoms fraction compared with the uniform sinogram assumption, and less than 1% error in the estimated NECR.

Usually some portion of the carbon fiber pallet of the patient table is in the field of view. The attenuation-correction-factor thresholding technique cannot distinguish this pallet from the

patient's body, causing this portion of the sinogram to be erroneously included in the mask defining the patient's interior. This causes the randoms to be overestimated by 5%–10% typically, and the scatter by about half that much. As a consequence, our estimates of clinical NECR are likely biased downward by 3%–5%.

Clinical Examples

To illustrate the application of the methodology, we present results for 2 patient populations: one that was scanned on the original LSO PET/CT scanner and the other on the LSO PET/CT scanner with Pico-3D digital electronics. *Pico-3D* refers to a new generation of fast, digital PET-processing electronics with improved time and energy resolution and reduced dead time (*19*). The newer system reduces the coincidence time window from 6 to 4.5 ns, with a proportional reduction in randoms, and improves the energy resolution from 23% to 19% (full width at half maximum at 511 keV), enabling the lower-level discriminator to be raised from 350 to 400 keV, thereby reducing scatter. Peak NECR measured according to the NEMA NU 2-2001 standard has been increased by a factor of 2, to approximately 100,000 cps, for the newer machine. Both scanners use an 8×8 LSO block detector with $6.7 \times 6.7 \times 25$ mm crystals and are otherwise similar. Neither scanner has interplane septa.

Two groups of ^{18}F-FDG whole-body studies were compared. Thirty-two patients (163 bed positions) were scanned on a Pico-3D machine (University of Tennessee Medical Center and Cleveland Clinic Foundation). Patient weight ranged from 37 to 135 kg, with a mean of 84 kg. Nineteen of the patients were male, and 13 female. Four patients were scanned with arms down, and the remainder with arms up.

Twenty-nine patients (also 163 bed positions) were scanned on a non–Pico-3D machine (Royal Prince Alfred Hospital). Patient weight ranged from 40 to 130 kg, with a mean of 88 kg. Twenty of the patients were male, and 9 female. Twenty patients were scanned with arms down, and the remainder with arms up.

Head and neck scans were excluded for both populations because NECR tends to be much higher for these than for scans elsewhere in the body. To some extent, imaging of the head and neck therefore constitutes a distinct situation deserving separate study. For both machines, counting-rate models were based on measurements performed on the NEMA NU 2-2001 70-cm phantom, which is intended to be used to characterize the performance of PET tomographs in the context of whole-body scanning (*6*). To evaluate its efficacy for this purpose, we included the phantom measurements in the analysis of our patient data as if the phantom were a 21.5-kg human. In principle, 1 point on each counting-rate curve (as we have for the patients) should be sufficient, but we included 20 points for each machine, spanning the clinical range of activities (approximately 25–500 MBq) to characterize the accuracy of the models with respect to fitting the counting-rate data. We also considered how closely the phantom's NECR response simulates that of patients if the phantom's activity concentration is simply scaled by the patient's weight (which is approximately proportional to volume), a technique that has frequently been used to infer clinical doses for human whole-body studies.

Anonymous patient data were selected mainly from prior routine clinical ^{18}F-FDG oncology studies and also from prior research studies approved by the affiliated Institutional Review Boards.

RESULTS

In Figure 2, we show plots of NECR(D_{inj}^{60}) for a randomly selected sample of 40 scans from each population, for the 1*R* case. Also shown for each machine are 2 NECR response curves for the NEMA NU 2-2001 70-cm phantom. For the first (the one peaking at lower dose), the dose was computed using the known total activity present in the 21.5-kg phantom, decay corrected by a factor of 1.46 for a 60-min uptake. For the second, an effective D_{inj}^{60} was computed from the decay-corrected activity concentration at each point by multiplying it by 70 L, the assumed volume of an average (70-kg) person, resulting in doses larger by a factor of 3.26 than for the first curve.

To better evaluate the variation in shape of the NECR response functions among scans, we scaled them on both the ordinate and the abscissa. In Figure 3 SNR/SNR_{max} versus D_{inj}^{60}/D_{max} is plotted for all 163 scans on the conventional LSO PET/CT scanner, for the 1*R* case. D_{max} is the value of D_{inj}^{60} at which SNR_{data} achieves its maximum, SNR_{max}. The corresponding curves for the Pico-3D and 2*R* cases (not shown) are likewise closely grouped, though of slightly different shapes. A remarkable feature of these curves is their broad, flat peaks. At least for long-lived isotopes such as ^{18}F ($t_{1/2}$ = 110 min), more efficient use of dose is clearly achieved by imaging patients at doses well below the peak of the response curve. For example, a 41% (for 1*R* or 44% for 2*R*) reduction in dose from its peak value reduces SNR_{data} by only 5% for the conventional system. We have thus chosen to evaluate the conventional system at an operational point of 95% of SNR_{max} for the following analyses. For the Pico-3D system, because of its higher dose requirements, we have chosen an operational point of 90%

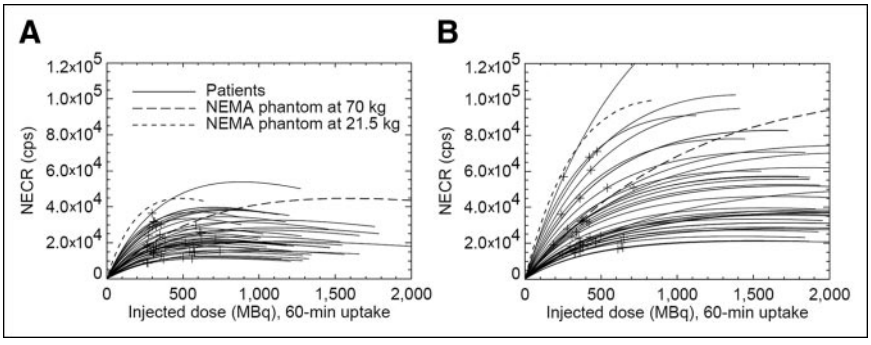

FIGURE 2. Plots of estimated patient-specific NECR (1*R* case) vs. D_{inj} for 40 clinical scans: conventional LSO PET/CT scanner (A) and Pico-3D LSO PET/CT scanner (B). Symbols indicate actual scan point. Dashed curves correspond to NEMA NU 2-2001 70-cm phantom.

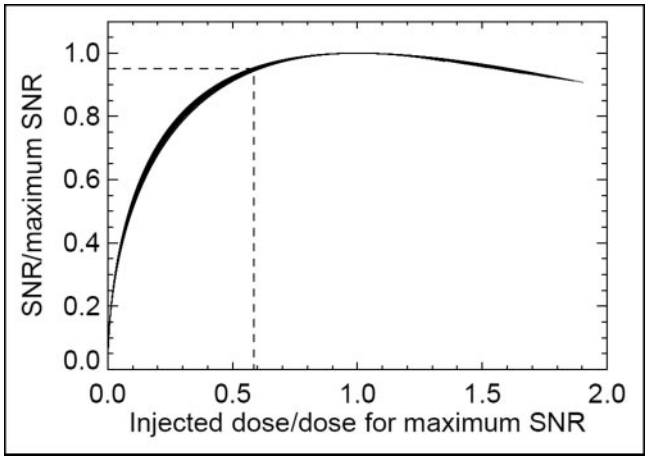

FIGURE 3. Relative response curves for 163 scans on conventional LSO PET/CT scanner, obtained by scaling SNR (1*R* case) and D_{inj} by their values at peak response.

of SNR_{max}, which permits dose to be reduced by 57% (for 1*R* or 61% for 2*R*).

For each patient scan, the optimal (90%–95% SNR_{max}) dose and NECR at this dose are determined. This optimal NECR is plotted versus patient weight in Figure 4 for both the 1*R* and 2*R* cases. Also shown in this and succeeding figures are the results for the NEMA phantom, represented by the points plotted at 21.5 kg. The trend lines are computed using only the patient data however. Optimal (90%–95% SNR_{max}) dose is plotted versus patient weight in Figure 5 for both the 1*R* and the 2*R* cases.

A better understanding of the trends in NECR and optimal dose with weight can be obtained by examining the various components of the data individually. In Figure 6A, we display the computed internal scatter fractions for the 2 patient populations versus weight. Figure 6B shows the corresponding trend for the internal randoms fractions, estimated as the fraction of the total delayed coincidences contained in LORs passing through the patient's body. Figure 7 shows the trends for the individual true, random, and scatter rates, summed over internal LORs, versus weight. These rates are evaluated at the optimal D_{inj}^{60} point (1*R*) for each patient scan, thereby reducing the confounding influence of arbitrarily varying activity levels. In Figure 7D we plot the ratio of the random and true coincidences.

DISCUSSION

We can see from Figure 2 that the NEMA phantom's response curves in fact do not match our typical patient response very well. The peak NECR value attained in the phantom is substantially higher than the mean patient value, and more important, when scaled to 70 kg using the activity concentration, the dose at which this peak value is attained is much higher for the phantom than for the patients, especially in the Pico-3D case. These results are consistent with the observations of Badawi et al. (*7*) and suggest that it is inappropriate to extrapolate this phantom's response to adult humans simply by scaling the activity concentration.

It appears from Figure 2 that there is a wide variety of distinct response curves for the different patients and bed positions. However, when rescaled as in Figure 3, it becomes clear that the relative response curves are similar for all studies on a particular machine type. This result is perhaps not too surprising considering that there are only 2 distinct trends for the component data, but it does suggest that the relative contributions from randoms and trues are not varying widely in the clinical counting-rate regime. The response shapes for the conventional and Pico-3D systems are similar, although the Pico-3D SNR_{data} tends to rise somewhat faster and fall less quickly above the peak because of its reduced dead time. For shorter-lived isotopes such as ^{82}Rb ($t_{1/2}$ = 76.4 s), ^{15}O ($t_{1/2}$ = 122 s), or ^{11}C ($t_{1/2}$ = 20 min), the broad region of near-optimal response is advantageous for increasing integral NECR as the activity decays, because relatively high doses may be used with little loss of data quality.

The phantom results in Figure 4 seem consistent with what we might expect for a 21.5-kg patient. Dispersion is negligible among the 20 sample points along the counting-rate curves for the phantom, confirming that we have adequately modeled these functions. The multiple points at a given patient weight represent the different bed positions for a single patient or, in some cases, the different scans for 2 or more patients having the same weight. For the Pico-3D population there are 5 weights that correspond to 2 patients

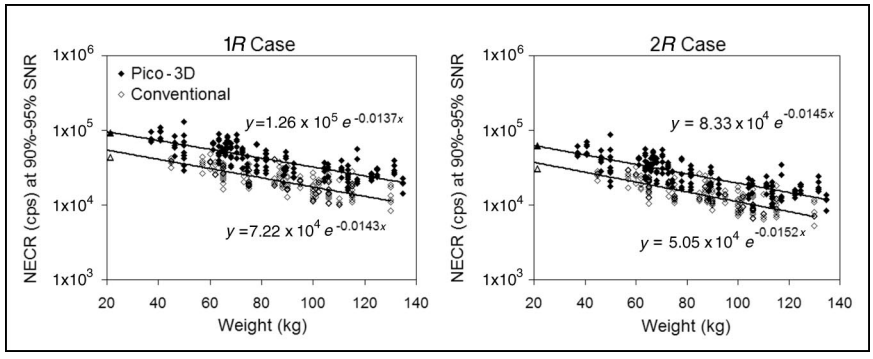

FIGURE 4. Plots of estimated NECR values at 90% or 95% of peak SNR, versus patient weight, for all scans. Fitted trend lines are also shown; each equation is associated with the nearest trend line. Points at 21.5 kg represent NEMA NU 2-2001 70-cm phantom data (not included in regression calculation).

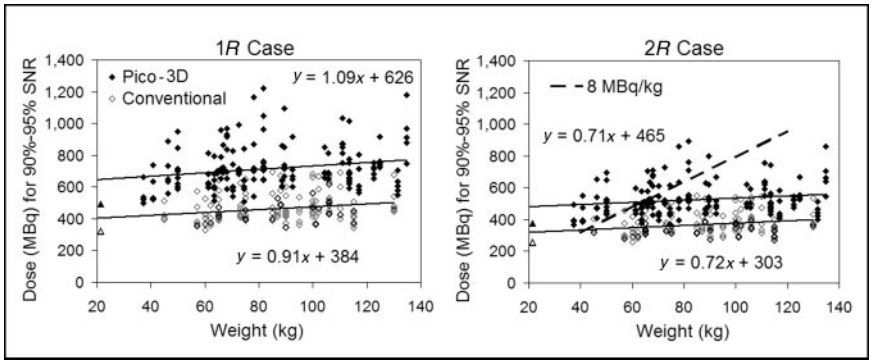

FIGURE 5. Plots of estimated optimal dose vs. patient weight for all scans, standardized to 60-min uptake. Dose is evaluated at 90% (Pico-3D) or 95% (conventional) of peak SNR. Dashed line in graph for 2R case corresponds to injection protocol of 8 MBq/mL.

each (50, 63.5, 68, 82, and 113 kg), whereas for the conventional population there are 3 weights corresponding to multiple patients (65, 75, and 100 kg). Thus, optimal NECR varies widely with position in the body as well as among different patients having the same weight.

Despite the dispersion due to body position and other factors, Figure 4 makes clear that NECR decreases rapidly with increasing patient weight. On average, NECR decreases about 1.4%–1.5% per additional kilogram. For example, using the equation for the Pico-3D 1*R* trend line from Figure 4A, $NECR(w) = 1.26 \times 10^5\ e^{-0.0137w}$, an increase in weight (w) from 60 to 120 kg implies a reduction by a factor of 0.44 in NECR, or a factor of 0.66 in mean SNR_{data} (recalling that SNR_{data} is proportional to the square root of NECR), for a fixed scan time. Thus, for equivalent SNR_{data}, a 120-kg person would have to be scanned 2.3 times longer than a 60-kg person. This strongly suggests the importance of making acquisition time dependent on weight in clinical protocols, as others have also suggested (*20*). Equalizing SNR_{data} between 2 weights does not necessarily imply that image quality would be comparable, however.

Pico-3D electronics improves SNR_{data} by 35% (for 1*R* and 32% for 2*R*) for a 70-kg person when optimal D_{inj}^{60} is used. Recall that we are computing Pico-3D results at 90% of maximum SNR but non-Pico results at 95% of maximum SNR. For a typical clinical dose of 370 MBq, rather than optimal dose, the improvement in SNR_{data} with Pico-3D at 70 kg is still significant (17% for 1*R* or 21% for 2*R*). Comparing 1*R* to 2*R* at optimal dose for a 70-kg patient, we find that 1*R* randoms processing would yield an increase in SNR_{data} of 26% (for Pico-3D or 23% for non–Pico-3D). At higher patient weights, the advantage of Pico-3D electronics or 1*R* data processing is somewhat greater because of their effectiveness in reducing randoms. For example, at 130 kg, Pico-3D electronics give an increase in SNR_{data} of 37% (for 1*R*) compared with non-Pico, whereas 1*R* processing improves SNR_{data} by 30% (for Pico-3D) compared with 2*R*.

The dispersion in the optimal dose, shown in Figure 5, with position in the body and other factors is apparently much greater than its average variation with patient weight. In fact, it appears that the average optimal dose increases only slightly (0.7–1.1 MBq/kg) with weight, suggesting that poorer image quality in larger patients generally cannot be overcome by increasing D_{inj} significantly in proportion to patient weight. This result is in contrast to some recent studies of clinical image quality (*21–23*). Using an LSO-based ECAT ACCEL dedicated PET scanner with conventional electronics (Siemens Molecular Imaging) that has a counting-rate response similar, though not identical, to that of the LSO PET/CT described here, Everaert et al. (*21*) found that ≥8 MBq of ^{18}F-FDG D_{inj} per kilogram was required to achieve good clinical image quality in a patient population 44–120 kg in weight. Halpern et al. (*22*), using an LSO PET/CT with conventional electronics and a D_{inj} rate of 7.77 MBq of ^{18}F-FDG per kilogram, found no variation in lesion detectability with weight for patients weighing 41–102 kg, for scan durations 2 min or longer. In a more recent study (*23*) of patients weighing 91–168 kg,

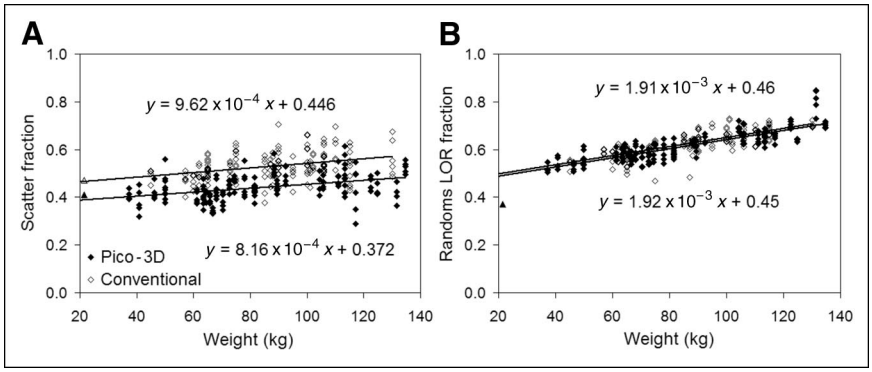

FIGURE 6. (A) Estimated internal scatter fraction for each scan vs. patient weight. (B) Randoms LOR fraction (fraction of total delayed coincidences estimated to lie on LORs passing through patient).

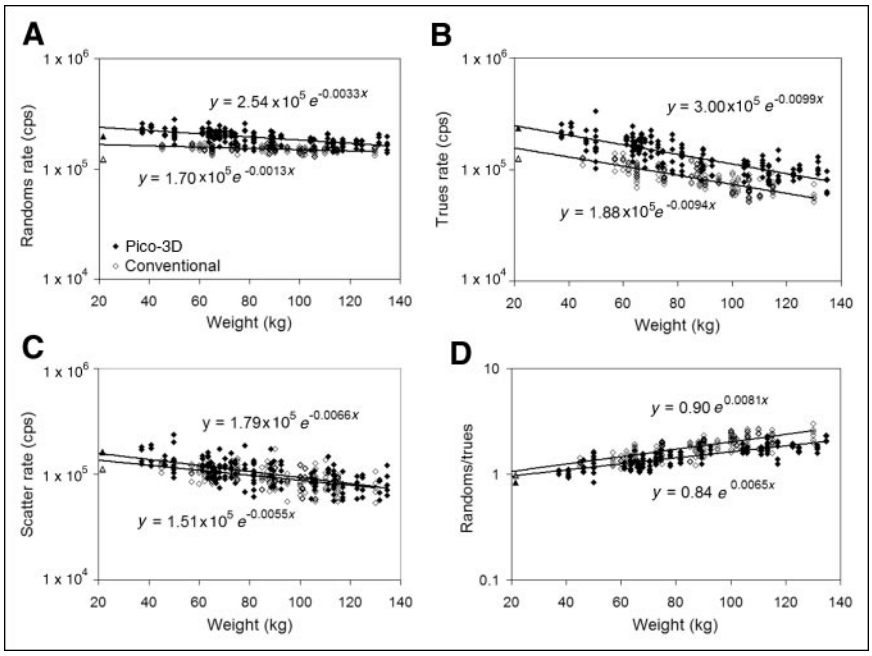

FIGURE 7. Estimated internal randoms (A), trues (B), and scatter (C) rates at 90% or 95% of SNR_{max} operation point for each study (1*R* case), plotted vs. patient weight. (D) Ratio of randoms to trues for each study.

they found no variation in detectability with weight for scans of 5 min or longer, again with 7.77 MBq of ^{18}F-FDG D_{inj} per kilogram (limited at 740 MBq). In all these studies, the nominal uptake period was 60 min and the randoms processing method was online randoms subtraction or its equivalent (the 2*R* case). The D_{inj}^{60}-versus-weight trend corresponding to 8 MBq/kg has been plotted as the dashed line in Figure 5B. Although this protocol seems compatible with our results for the lightest patients, we believe that heavier patients would realize little benefit on average from the much higher D_{inj} implied by this recipe.

We observed significant variation in optimal dose with position in the body. Notwithstanding the possibility that this apparent variability could be partly due to coincidental factors, imaging that is targeted to a specific region of the body could well require a very different dose from the dose that is best for a whole-body survey on average. On the other hand, a possible strategy for whole-body scans would be to inject doses closer to the maximum optimal dose for any bed position, rather than doses closer to the mean optimal dose over all bed positions.

Pico-3D mean optimal dose over all weights is 717 MBq (for 1*R* or 524 MBq for 2*R*) versus 464 MBq (for 1*R* or 366 MBq for 2*R*) for the conventional system. Again, the points at 21.5 kg in Figure 5 are from the NEMA phantom measurement. Optimal doses for this phantom are perhaps somewhat lower than one would extrapolate from the patient data, but on the other hand the phantom dose does not allow for partial excretion as is common in patients. Table 1 summarizes the performance differences between the conventional and Pico-3D LSO PET/CT scanners as determined from our clinical analyses.

Mean scatter fraction (Fig. 6A) increased only moderately (about 20%) over the entire range of patient weight examined (35–135 kg). The variation among the different positions in the body is comparable to or greater than this. We speculate that scatter may be mitigated to some extent for larger patients by the self-shielding effect of their own bodies, which may limit contributions from outside the field of view of the scanner. Thus, while increasing scatter fraction contributes to the degradation of SNR with increasing weight, as has been suggested by other workers (*20,24*), it does not seem to be the dominant factor. The main reason the conventional electronics exhibit a larger scatter fraction than does the Pico-3D system is that a lower value for the lower-level discriminator for the energy qualification window is used: 350 keV compared with 400 keV. Interestingly, the scatter fractions for the NEMA phantom are quite consistent with the patient data even though they are computed in very different ways: The NEMA scatter fraction is

TABLE 1
Comparison of Clinical Performance Results for Conventional and Pico-3D Digital Electronics

Metric	Conventional		Pico-3D	
	1*R*	2*R*	1*R*	2*R*
Peak patient NECR (at 70 kg; kcps)	29.4	19.3	59.6	37.3
NECR at optimal dose (at 70 kg; kcps)	26.5	17.4	48.3	30.2
NECR at 370 MBq (at 70 kg; kcps)	24.7	17.6	33.9	25.9
Mean optimal dose (MBq)	464	366	717	524
Mean scatter fraction	0.53	0.53	0.44	0.44
Mean ratio of randoms to trues	1.87	1.54	1.50	1.14

estimated by interpolating a background beneath a line source profile, whereas the patient scatter fraction is computed via simulation.

The randoms fraction shown in Figure 6B has a more significant weight trend (36% increase from 35 to 135 kg), as we might expect because of the increasing volume of patients as their weight increases, but dispersion due to position in the body is less than for the scatter fraction. The NEMA 70-cm phantom has a low randoms fraction compared with the patient trend, because of its long, thin geometry. In this case, the bed pallet is excluded from the definition of the object for the purpose of determining randoms and scatter fractions, but this is partly compensated by the NEMA-specified inclusion of a 2-cm radial annulus adjacent to the cylinder.

The individual true, random, and scatter rates shown in Figure 7 all generally decrease with weight. The randoms rates for the NEMA phantom are substantially less than what we would extrapolate for a 21.5-kg patient, largely because of its low randoms fraction. From Figure 7D, we see that for optimal operation *R*/*T* is nearly always greater than 1. Although the Pico-3D system has a more favorable ratio, both systems show a marked increase in *R*/*T* with increasing weight. Over the weight range considered, *R*/*T* increases by about a factor of 2.

A major factor in the degradation of SNR_{data} with increasing weight appears to be the loss of true coincidences, as seen in Figure 7B. The trues decrease much more rapidly than the randoms as weight increases (in fact, by more than a factor of 2.5 over the range shown), likely as a consequence of their increased attenuation by the larger bodies. The randoms may be less sensitive to this increased mass because their requisite total pathlength through the body is less than that for true coincidences. Further, the growing randoms fraction due to the larger volume of heavier patients counteracts the effect of the decreasing singles rate to some extent. There is also a significant contribution to the singles from the intrinsic radiation in the LSO detectors that does not vary with patient weight and tends to moderate the randoms variation.

An analysis of the sensitivity of NECR at optimal dose to small independent changes in the various component counting rates shows that it is numerically most sensitive to the loss of trues as patient weight increases. However, changes in scanner design or operational parameters generally affect the scatter, randoms, and trues rates in a coupled way, and knowledge of these tradeoffs is required to optimize scanner performance.

CONCLUSION

We have described a new method for accurately estimating the variation of true, random, and scatter coincidence rates with D_{inj} in clinical PET by means of a simple scaling of the phantom-derived trues and randoms rate functions to the actual measured values. When combined with the accurate estimates of scatter and randoms fractions currently available, the $SNR(D_{inj})$ response specific to any individual acquisition can be computed. From this, one can retrospectively compute optimal dose and SNR_{data} for each scan. Such data, when correlated with anatomy, weight, and other patient characteristics, could potentially be used to prospectively choose appropriate doses for individual scans.

Significant improvement in clinical counting-rate performance is observed with the Pico-3D digital electronics system because of its reduced dead time and improved ability to reject randoms and scatter.

In most respects, the responses of the scanners to the NEMA NU 2-2001 70-cm phantom closely resemble those expected for a 21.5-kg human subject. Scaling its activity concentration by patient weight is not an accurate way of inferring appropriate doses for heavier patients, however.

For longer lived isotopes such as ^{18}F, dose is much more efficiently used when scanning is performed at 90%–95% of peak SNR, on the machines considered here. The variation in this optimal dose with patient weight appears to be small, on average, although the variation with position in the body is much larger.

We find that peak SNR_{data} decreases rapidly with patient weight, indicating that the only way to maintain data quality for larger patients is to scan longer. As patient weight increases, fewer photons are getting out of the body at optimal D_{inj}, and a higher fraction of these are randoms and, to a lesser extent, scatter. Thus, counting losses are less important but higher sensitivity and improved randoms noise reduction techniques are likely more important for heavier patients than for lighter ones.

REFERENCES

1. *NEMA Standards Publication NU 2-2001: Performance Measurements of Positron Emission Tomographs.* Rosslyn, VA: National Electrical Manufacturers Association; 2001.
2. Bailey DL, Jones T, Spinks TJ, et al. Noise equivalent count measurements in a neuro-PET scanner with retractable septa. *IEEE Trans Med Imaging.* 1991;10: 256–260.
3. Dahlbom M, Cherry SR, Eriksson L, et al. Optimization of PET instrumentation for brain activation studies. *IEEE Trans Nucl Sci.* 1993;40:1048–1054.
4. Stearns CW, Cherry SR, Thompson CJ. NECR analysis of 3D brain PET scanner designs. *IEEE Trans Nucl Sci.* 1995;42:1075–1079.
5. Badawi RD, Marsden PK, Cronin BF, et al. Optimization of noise-equivalent count rates in 3D PET. *Phys Med Biol.* 1996;41:1755–1776.
6. Daube-Witherspoon ME, Karp JS, Casey ME, et al. PET performance measurements using the NEMA NU 2-2001 standard. *J Nucl Med.* 2002;43:1398–1409.
7. Badawi RD, Adam L-E, Zimmerman RE. A simulation-based assessment of the revised NEMA NU-2 70-cm long test phantom for PET. In: *2001 IEEE Nuclear Science Symposium and Medical Imaging Conference* [book on CD-ROM]. Piscataway, NJ: IEEE; 2001:M6–6.
8. Smith RJ, Karp JS. Comparisons of clinical performance with standard measures of PET cameras. In: *1998 IEEE Nuclear Science Symposium and Medical Imaging Conference* [book on CD-ROM]. Piscataway, NJ: IEEE; 1998:M6–11.
9. Lartizien C, Comtat C, Kinahan PE, et al. Optimization of injected dose based on noise equivalent count rates for 2- and 3-dimensional whole-body PET. *J Nucl Med.* 2002;43:1268–1278.
10. Watson CC, Casey ME, Beyer T, et al. Evaluation of clinical PET count rate performance. *IEEE Trans Nucl Sci.* 2003;50:1379–1385.
11. Watson CC, Casey ME, Michel C, Bendriem B. Advances in scatter correction

for 3D PET/CT. In: *2004 IEEE Nuclear Science Symposium and Medical Imaging Conference* [book on CD-ROM]. Piscataway, NJ: IEEE; 2004:M5–166.
12. Watson CC. Count rate dependence of local signal-to-noise ratio in positron emission tomography. *IEEE Trans Nucl Sci.* 2004;51:2670–2680.
13. Müller JW. Dead-time problems. *Nucl Instrum Methods.* 1973;112:47–57.
14. Badawi RD, Domigan P, Johnson O, et al. Count-rate dependent event mispositioning and NEC in PET. In: *2002 IEEE Nuclear Science Symposium and Medical Imaging Conference* [book on CD-ROM]. Piscataway, NJ: IEEE; 2002: M7–43.
15. Dahlbom M, Schiepers C, Czernin J. Comparison of noise equivalent count rates and image noise. In: *2004 IEEE Nuclear Science Symposium and Medical Imaging Conference* [book on CD-ROM]. Piscataway, NJ: IEEE; 2004:M9–303.
16. Stearns CW. Estimating an acquisition-specific NEC curve for PET acquisitions. In: *2003 IEEE Nuclear Science Symposium and Medical Imaging Conference* [book on CD-ROM]. Piscataway, NJ: IEEE; 2003:M10–205.
17. Erdi YE, Nehmeh SA, Mulnix T, et al. PET performance measurements for an LSO based combined PET/CT scanner using the NEMA NU 2-2001 standard. *J Nucl Med.* 2003;45:813–821.
18. Eriksson LE, Watson CC, Wienhard K, et al. The ECAT HRRT: an example of NEMA scatter estimation issues for LSO based PET systems. In: *2003 IEEE Nuclear Science Symposium and Medical Imaging Conference* [book on CD-ROM]. Piscataway, NJ: IEEE; 2003:M3–139.
19. Puterbaugh KC, Breeding JE, Musrock MS, Seaver CE, Young JW. Performance comparison of a current LSO PET scanner versus upgraded electronics. In: *2003 IEEE Nuclear Science Symposium and Medical Imaging Conference* [book on CD-ROM]. Piscataway, NJ: IEEE; 2003:M3–133.
20. Paans AMJ, Boerdijk SMM, Willemsen ATM, Pruim J. Source of impaired image quality in 3D whole-body FDG PET scanning [letter]. *Eur J Nucl Med Mol Imaging.* 2004;31:1207.
21. Everaert H, Vanhove C, Lahoutte T, et al. Optimal dose of ^{18}F-FDG required for whole-body PET using an LSO PET camera. *Eur J Nucl Med Mol Imaging.* 2003;30:1615–1619.
22. Halpern BS, Dahlbom M, Quon A, et al. Impact of patient weight and emission scan duration on PET/CT image quality and lesion detectability. *J Nucl Med.* 2004;45:797–801.
23. Halpern BS, Dahlbom M, Auerbach MA, et al. Optimizing imaging protocols for overweight and obese patients: a lutetium orthosilicate PET/CT study. *J Nucl Med.* 2005;46:603–607.
24. Everaert H, Vanhove C. Reply [letter]. *Eur J Nucl Med Mol Imaging.* 2004;31: 1208.